HOSTED BY
ELSEVIER
Available online at www.sciencedirect.com
ScienceDirect
Soils and Foundations 62 (2022) 101152
www.elsevier.com/locate/sandf

Technical Paper

Failure mechanism of fine-grained soil-structure interface for energy piles

Elena Ravera *, Lyesse Laloui

Laboratory of Soil Mechanics, École Polytechnique Fédérale de Lausanne, Station 18, CH 1015 Lausanne, Switzerland

Received 7 September 2021; received in revised form 7 March 2022; accepted 6 April 2022

Abstract

The response of the soil-structure interface can significantly affect the performance of any geotechnical structure. Thermal cycles are a new factor that influence the response to all structures that have an energy function in addition to the structural one, such as energy piles foundations. In this study, a theoretical interpretation of the failure mechanism at the pile-soil interface subjected to cyclic thermal loads and a dedicated constitutive model is presented. The phenomenon is characterised by large localised strains concentrated in a thin layer around the pile surrounded by soil behaving under oedometric conditions. The theoretical framework refers to direct shear tests at a constant normal stiffness, as well as oedometric tests on clayey soil. Observations indicate a negligible effect of the temperature cycles on the soil-structure interface response for typical temperature ranges of energy piles ($\Delta T = -10, +20$ °C). Therefore, an isothermal mathematical formulation in the framework of elastoplasticity is proposed for the analysis of both conventional and energy piles. The effectiveness of the interface model in reproducing the observed behaviour is confirmed via experimental tests. The proposed constitutive model is applicable in engineering practice via the finite-element or the load-transfer method. Additionally, its calibration requires exclusively conventional geotechnical testing.

Keywords: Energy piles; Soil-concrete interface; Thermomechanical behaviour; Fine-grained soil; Constitutive model

1. Introduction

The analysis of energy pile foundations requires—as a starting point—an estimate of the capacity of a single pile to withstand a mechanical load, given its primary structural support functions, and the thermal load associated with the heat-exchanger functions. In assessing the capacity of the energy pile, the shaft resistance represents the main contribution to the axial capacity. The shearing behaviour of the soil-structure interface governs the response of pile foundations. Therefore, understanding the soil-structure interface behaviour is critical for determining the load-transfer for foundations such as axially loaded piles. For conventional axially loaded piles, the importance of the interface zone as a transfer zone was highlighted by Randolph (2003) and Pra-ai and Boulon (2017). Early studies on the elementary mechanism of the mobilisation of the shaft resistance at the pile-soil interface were performed by Boulon and Foray (1986). They concluded that the direct shear test is representative of the mechanism that occurs at the pile-soil interface under real conditions. Experimental studies on direct shear tests on fine-grained soil-structure interface were presented by Potyondy (1961), Littleton (1976), Tsubakihara and Kishida (1993), Ovando-Shelley (1995), Shakir and Zhu (2009) and Feligha et al. (2016). Three typical boundary conditions are generally used in such laboratory experiments: (i) a

Peer review under responsibility of The Japanese Geotechnical Society.
* Corresponding author.
E-mail addresses: elena.ravera@epfl.ch (E. Ravera), lyesse.laloui@epfl.ch (L. Laloui).

https://doi.org/10.1016/j.sandf.2022.101152

constant normal stress (CNL), (ii) a constant volume, (iii) and a constant normal stiffness (CNS). Condition (iii) takes account for the effects of the volume changes that occur as soil adjacent to a pile is sheared (Tabucanon et al., 1995). The volumetric response of the soil at the interface is not completely free to develop. The response is partially prevented by the presence of the surrounding soil, which acts as a spring on the interface. The spring stiffness replicates the far-field stiffness around a cylindrical pile and is generally assumed to be constant, implying an elastic soil response (DeJong et al., 2006). The value of the stiffness is derived from the use of the cylindrical cavity expansion theory and is a function of the shear modulus of the soil at small deformation and the radius of the pile. When it is 0 corresponds to the CNL condition. In the case of fine-grained soils these values are relatively low as the shear modulus is lower than in coarse-grained soils (Di Donna et al., 2016). Consequently, the normal stress acting on the interface may increase or decrease as a result of the dilative-contractive behaviour at the pile soil interface (Fakharian and Evgin, 1997). Over the past three decades, significant advances in the direct shear testing of interfaces have been made. CNS tests have been recognised as a suitable laboratory tests for tracking the effects of interface volume changes and dilatancy, particularly when cyclic loading is applied (Poulos, 2017). Information obtained from laboratory CNS tests—under both static and cyclic loading—was used in the foundation design for the Emirates Twin Towers, Dubai (Poulos and Davids, 2005). The values of the ultimate shaft friction along the pile inferred from the load tests agreed well with the values used for design, which were derived from CNS laboratory tests. These results indicate the potential of this type of test for accurately measuring the pile shaft friction characteristics in the laboratory (Poulos and Davids, 2005).

In energy pile foundations, the response of an energy pile–soil interface is influenced by seasonal and daily cyclic thermal variations. Such physical processes should be considered in the analysis of the behaviour of soils as well as soil-concrete interfaces. Lancellotta and Ruiz (1999) and Fleming et al. (2008) reported that an effective stress approach is nowadays considered to estimate the shaft capacity of piles for both coarse- and fine-grained soil. According to this consideration, the parameters included in the shaft capacity formulation are (i) the pile-soil interface angle of the shear strength, which can be approximated as the soil angle of the shear strength under constant volume conditions, and (ii) the normal effective stress acting on the pile shaft. Thus, in the context of energy piles, there is a need to understand the effect of the temperature on the two parameters that govern the pile-soil shear strength. With regard to fine-grained soil behaviour, for which a relatively high sensitivity to temperature variations has been historically observed, extensive studies have been performed on clay for different thermal paths (Hueckel and Pellegrini, 1989; Hueckel and Baldi, 1990; Robinet et al., 1997; Burghignoli et al., 2000; Graham et al., 2001; Cekerevac and Laloui, 2004; Ghahremannejad, 2003; Yavari et al., 2016; Li et al., 2019; Maghsoodi et al., 2020) and, only recently, on clay-structure interfaces (Di Donna et al., 2016; Yavari et al., 2016; Li et al., 2019; Yazdani et al., 2019; Maghsoodi et al., 2020; Ravera et al., 2021). The results indicate that the temperature has a negligible influence on the angle of the shear strength. In addition, the new results presented in Ravera et al. (2021) highlighted a negligible variation of the normal stress acting on the pile shaft in relation to thermal actions based on tests in which both CNS conditions and cyclic thermal load are applied together.

This study presents a theoretical interpretation and a constitutive model, validated on the experimental results presented in Ravera et al. (2021), for the interpretation of the shear response of the soil-structure interface in energy piles applications. The interpretation of the direct shear test is based on the idealisation of the interface as a surface. Originally proposed by Boulon (1989) for conventional piles, it is herein proposed in the context of energy piles. The soil sample is schematically decomposed in a sheared interface, and an oedometric sample that acts as a restraining elastic medium (Boulon, 1989; Ghionna and Mortara, 2002; Pra-ai and Boulon, 2017). The main findings and rheological evidence of the experimental data from oedometric tests and CNS direct shear tests presented in Ravera et al. (2021) are summarised in the essential features to support the theoretical interpretation and the constitutive development. The basic failure phenomenon of the soil-structure interface of energy foundations is described by an elastoplastic constitutive model. The model is used to predict the results of CNS direct shear tests by using only the results of standard oedometer and CNL direct shear tests. In addition, the proposed constitutive model has the advantage and novelty of being developed under the framework of the Mohr-Coulomb elastoplastic models. This makes it more attractive and usable for engineering analysis and distinguishes it from the current models available.

2. Element test

The direct shear test is considered to be the most suitable type of test for experimentally reproducing the soil-structure interface behaviour (Boulon and Foray, 1986; Boulon, 1989; Boulon and Nova, 1990; Boulon et al., 1995; Ghionna and Mortara, 2002; Pra-ai and Boulon, 2017). This test assesses both the dilatancy aspects and the characteristics of the discontinuity surface. In the case of a pile foundation, large localised strains are concentrated in a thin layer around the pile (Boulon et al., 1995; Ghionna and Mortara, 2002). Among the boundary conditions, i.e., the (i) CNL, (ii) constant volume, and (iii) CNS, the last one is recognised as the most appropriate for reproducing the basic mechanism of the mobilisation of the shaft resistance at the pile-soil interface. Some concerns of direct shear testing relate to the homogeneity of the test. However, observations of non-homogeneity arise from the use

of a continuum approach. Considering the test as a surface test, homogeneity should only occur in the shear band (Boulon, 1989).

A theoretical interpretation of the soil-structure interface behaviour was proposed by Boulon (1989) where the interface is considered as a surface and replaced with a layer of zero thickness subjected to tangential and normal discontinuities. This is an efficient approach for modelling complex phenomena in a bidimensional manner (Boulon, 1989). According to these observations, the interpretation of the direct shear test proposed by Boulon (1989) divides the sample into the following two parts. (i) The interface, i.e., the lower part where the soil and the material representing the pile surface are in contact, is defined as the "active" part, and (ii) the "passive" part is the remainder of the soil above the interface under oedometric conditions.

A schematic of the soil sample in the direct shear device is shown in Fig. 1.

3. Rheological evidences

In light of the previous considerations, an experimental investigation was presented in Ravera et al. (2021) to obtain additional insight into the response of soil-concrete interface to thermal cycles for typical temperature ranges of energy piles ($\Delta T = -10, +20$ °C). It was necessary for the volumetric and shear responses to be individually studied to obtain an understanding of the coupled behaviour. Thus, the experimental program comprised cyclic thermal tests under a constant vertical effective stress in oedometric conditions and CNS direct shear tests, where the soil-concrete interface was subjected to thermal cycles. Specifically, monotonic shearing was performed under CNS conditions at ambient temperature after the application of cyclic thermal loads under CNS conditions. In the following the focus is on the samples of clayey soil under normally consolidated conditions because from the rheological evidence in the literature these are the ones that could determine a greater variation of the normal stresses with a consequent effect on the shear strength of the piles

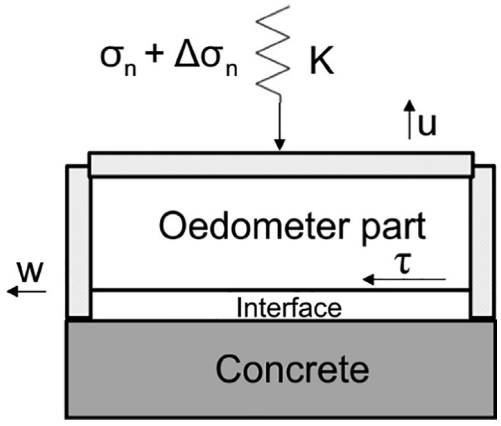

Fig. 1. Interpretation of the direct shear test.

(Laloui and Rotta Loria, 2019; Rotta Loria and Coulibaly, 2020; Ravera et al., 2021). In this study the main specifications and results are presented to support the understanding of the theoretical interpretation and the constitutive model.

Oedometric results (Fig. 2(a)) highlighted that the cyclic volumetric response of fine-grained soil to thermal cycles is mainly reversible. When this is contextualised in the theoretical interpretation of the behaviour at the interface, reversible behaviour indicates that the boundary conditions of the interface are not changed by the temperature cycles. The stiffness exerted on the interface by the oedometric part of the sample remains unchanged after the application of thermal cycles.

Constant normal stiffness direct shear tests (Fig. 2(b)) provide indications regarding the likelihood of the degradation of the shear strength of the pile under a cyclic thermal load. Indeed, shear strength is by its definition a function of normal stress (to the plane, where it is considered) and reducing normal stress from an elastic state may lead to failure (like in cyclic mobility failure). No significant difference in the shear response behaviour of the interface after thermal cycles has been observed by Ravera et al. (2021) compared to a purely mechanical stress path. The application of the thermal load had a minimal effect (or no effect) on the shear stress in the shearing phase. This implies that the failure envelope remained practically unchanged.

Based on the observations described in Ravera et al. (2021), the volume change did not significantly affect the shear resistance under the investigated conditions, i.e., no significant changes in the effective normal stress during the thermal cycles were noted (Ravera et al., 2021) indicating a negligible effect of the temperature at the interface. On the basis of the rheological evidence discussed above, a constitutive model is proposed below for studying the interfaces of both conventional and energy piles.

4. Soil-structure interface model

The equivalent continuum theory is not applicable to mechanisms that involve large relative displacements between the grains or large rotations of the grains, e.g., when the soil-structure interface is sheared. Therefore, specific interface constitutive equations are needed to numerically simulate the soil-structure interaction in cases where localised large displacements are expected (Boulon and Nova,1990). To model the fundamental aspects of the shearing behaviour of an interface, a representative constitutive model must represent the different responses of the element being analysed in relation to the path and type of load. The previously described experimental results suggest a negligible effect of the temperature. Therefore, a mathematical formulation independent of this variable is considered.

A pragmatic approach adopted by Boulon (1989), Boulon and Nova (1990), and Ghionna and Mortara

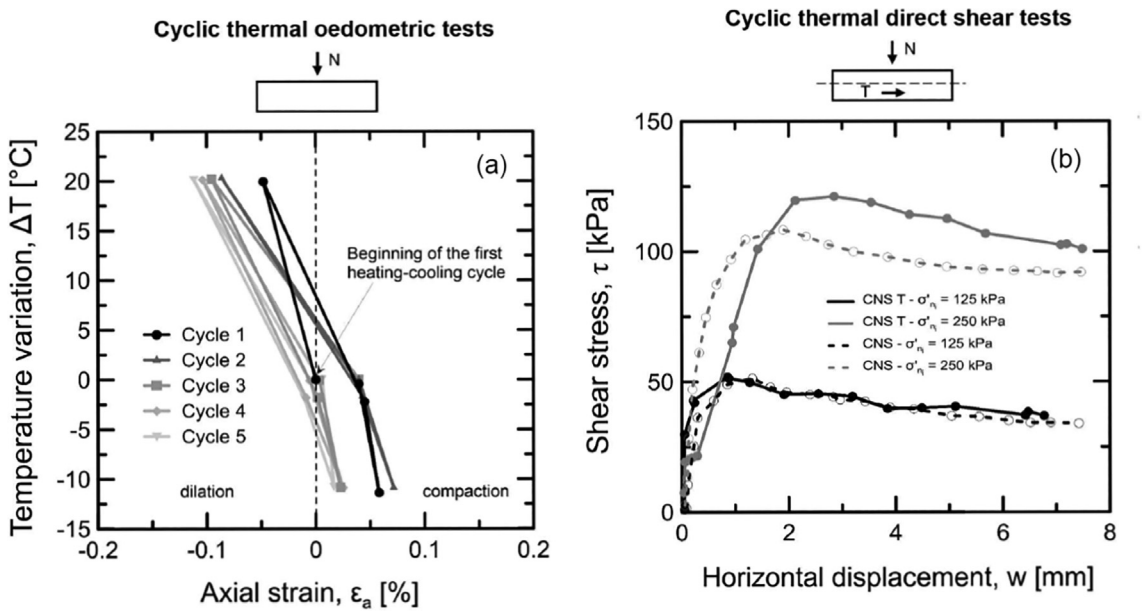

Fig. 2. (a) Thermal axial strain of a normally consolidated clayey soil during drained heating–cooling cycles (initial consolidation pressure of 125 kPa). (b) Results of clay-concrete interface tests under CNS conditions. Comparisons between isothermal (CNS) and cyclic thermal tests (CNS T)(modified from Ravera et al. (2021)).

(2002) involves idealising the soil-structure interface as a surface and thus as a bidimensional continuum. The interface is replaced by a zone of zero thickness where kinematic discontinuities occur. This idealisation can be used to model the complex phenomena occurring between the two boundaries of a shear band inside the soil adjacent to a structure (Boulon, 1989). Using this approach, the model was formulated with the interface stress and displacement. Hereafter, the development of an interface model for simulating the failure mechanism along the inclusion in the soil is presented.

4.1. Elastoplastic framework for soil-structure interface behaviour

The mathematical model of the interface behaviour presented herein employs the concepts of elastoplasticity. The objective was to develop an elastoplastic model for interfaces between soil and rigid inclusions. Elastoplastic models for interface behaviour have been proposed by Boulon and Nova (1990) and Ghionna and Mortara (2002). A similar approach was used in this study. The model presented herein is based on the extended Mohr-Coulomb model with the hardening model presented by Wood (2004), which is generally used for triaxial tests. The choice of the model is based on the need to provide engineers with a suitable tool for geotechnical problems. Thus, Mohr Coulomb models are commonly used; additionally, engineers are more likely to use models that they are familiar with (Wood, 2004). The description of the model presented by Wood (2004) refers to conditions that are accessible in the conventional triaxial apparatus. The behaviour observed in the triaxial device can be compared equivalently to the behaviour observed in the shear device; a direct analogy can be drawn between the strain increments and the displacement increments and between the effective stresses and the loads (Wood, 2004). Thus, there is a formal correspondence between p', q, ε_p, and ε_q in a triaxial test and between σ'_n, τ, u, and w in a direct shear test. Finally, in both cases, models with the same mathematical structure can be employed, except for the choice of appropriate variables (Boulon & Nova, 1990).

The formulations of the main components of the model are rewritten below for the bidimensional case and with reference to the variables of the direct shear test. Using an elastoplastic framework, the underlying assumption is that the displacement increments can be divided into elastic (^{e}) and plastic (^{p}).

$$\delta u = \delta u^e + \delta u^p \tag{1}$$

$$\delta w = \delta w^e + \delta w^p \tag{2}$$

Here, δu represents the axial displacement, and δw represents the tangential displacement.

4.1.1. Elastic properties

Linear elastic behaviour is assumed, similar to the study of Ghionna & Mortara (2002).

$$\begin{bmatrix} \delta\sigma'_n \\ \delta\tau \end{bmatrix} = \begin{bmatrix} K_n & 0 \\ 0 & K_s \end{bmatrix} \begin{bmatrix} \delta u^e \\ \delta w^e \end{bmatrix} \tag{3}$$

The elastic properties are the normal stiffness, K_n, and the shear stiffness, K_s, which are proportional to a constant, C_K.

$$K_s = C_K K_n \tag{4}$$

This originates from the formulation of the model in terms of stress and displacement.

4.1.2. Yield function

The yield function identifies the region in the stress space where the behaviour is elastic. The criterion adopted in this study is

$$f\left(\sigma_n^{'},\tau,k\right)=\tau-k\sigma_n^{'} \tag{5}$$

where k is a hardening parameter that indicates the current size of the yield surface and is given by the maximum stress ratio $\tau/\sigma_n^{'}$ attained in the interface.

4.1.3. Flow rule

The flow rule is the ingredient of the hardening plastic model to describe the mechanism of plastic deformation (Wood, 2004). The proposed formulation is based on the precursor stress-dilatancy relationship presented by Taylor (1948).

$$\frac{\delta y}{\delta x}=\mu-\frac{Q}{P} \tag{6}$$

Here, δy represents the vertical (volumetric) displacement, δx represents the horizontal (shearing) displacement, Q represents the horizontal load, P represents the vertical load, and μ is a coefficient that expresses the frictional contribution. In this study, similar to the studies of Boulon and Nova (1990) and Ghionna and Mortara (2002), the stress-dilatancy relationship controlled the ratio of the plastic displacement increments. It can be expressed as

$$\frac{\delta u^p}{\delta w^p}=\mu-\frac{\tau}{\sigma_n^{'}} \tag{7}$$

Then, the flow rule is expressed as

$$\begin{bmatrix}\delta u^p\\ \delta w^p\end{bmatrix}=\lambda\begin{bmatrix}\frac{\partial g}{\partial \sigma_n^{'}}\\ \frac{\partial g}{\partial \tau}\end{bmatrix}=\lambda\begin{bmatrix}\mu-k\\ 1\end{bmatrix} \tag{8}$$

The corresponding non associated plastic potential function is as follows:

$$g(\sigma')=\tau-\mu\sigma_n^{'}ln\frac{\sigma_n^{'}}{\sigma_r^{'}} \tag{9}$$

where $\sigma_r^{'}$ is an arbitrary variable for generating plastic potential curves passing thorough the current stress state of this general class (Wood, 2004).

Fig. 3 shows the plastic potential curves, the yield functions, and the directions of the plastic displacement increment vectors.

4.1.4. Hardening rule

In this model, the hardening is related to the shear displacements only. Therefore, the normalised stiffness reduction is described by a hyperbolic relationship between the stress ratio and the shear displacements:

$$\frac{k}{k_p}=\frac{w^p}{a+w^p} \tag{10}$$

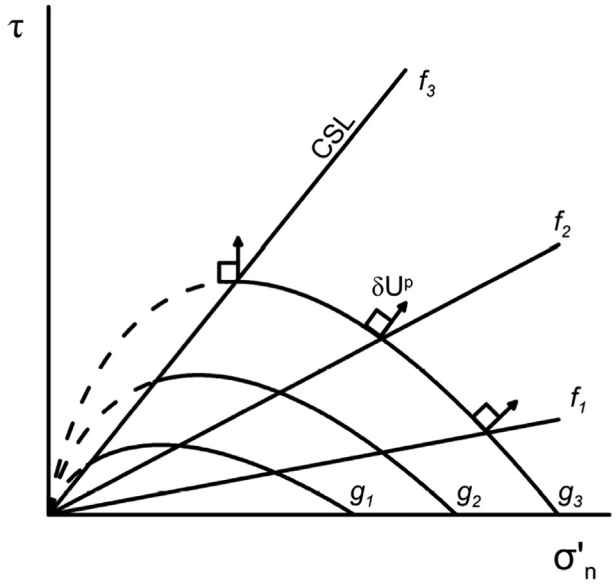

Fig. 3. Elastoplastic model for the interface: yield function (f_i); plastic potential curves (g_i).

where k_p is the upper limit of the stress ratio, and a is a soil constant. Equation (10) can also be written in incremental form:

$$\begin{bmatrix}\delta k/\delta u^p\\ \delta k/\delta w^p\end{bmatrix}=\begin{bmatrix}0\\ \frac{(k_p-k)^2}{ak_p}\end{bmatrix} \tag{11}$$

4.1.5. Model parameters

The elastic-hardening plastic model presented herein is characterised by five constitutive parameters, as shown in Table 1. These can be determined using the results of the standard CNL direct shear tests and standard oedometric tests.

4.1.6. Numerical integration of constitutive model

With the foregoing analytical functions, the elastoplastic problem can be expressed as follows:

$$\delta\boldsymbol{\sigma}=\left[\mathbf{D}^e-\frac{\mathbf{D}^e\frac{\partial g}{\partial\sigma}\frac{\partial f}{\partial\sigma}^T\mathbf{D}^e}{\frac{\partial f}{\partial\sigma}^T\mathbf{D}^e\frac{\partial g}{\partial\sigma}+H}\right]\delta\boldsymbol{U}=\mathbf{D}^{ep}\delta\boldsymbol{U} \tag{12}$$

where $\boldsymbol{\sigma}$ represents the stress vector, $\mathbf{D}^e$ represents the elastic stiffness matrix, H is the hardening parameter, $\mathbf{D}^{ep}$ represents the elastoplastic stiffness matrix, and $\boldsymbol{U}$ represents the displacement vector.

Table 1
Calibrated parameters for the predictive analyses.

Elastic parameters	
Normal stiffness [kPa/mm], K_n	*1500*
Shear stiffness [kPa/mm], K_s	*1500*
Plastic parameters	
Shear coefficient, μ	*0.47*
Limiting value of stress ratio, k_p	*0.442*
Soil constant, a	*0.02*

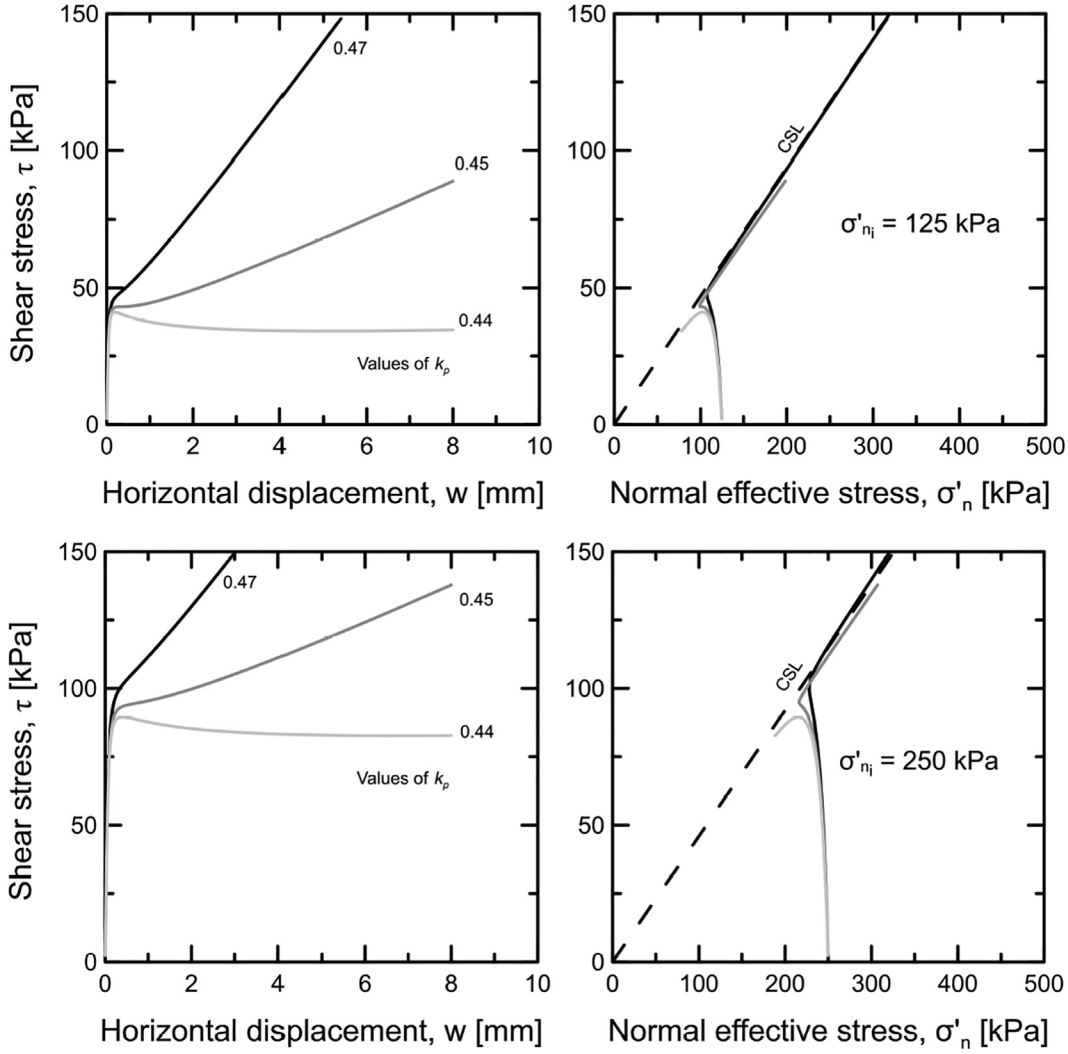

Fig. 4. Sensitivity analysis results for the parameter k_p.

The constitutive equation was integrated using a stress point algorithm. An explicit method with automatic substepping and error control presented by Sloan (1987) and Sloan et al. (2001) was used, as its reliability and efficiency for such models had been proven. Specifically, modified Euler integration with error control was adopted, and additional stress control was implemented to apply the CNS conditions (Appendix A).

4.2. Model application

4.2.1. Calibration tests

Calibration against laboratory tests was necessary for obtaining the parameters of the model. To define the performance appropriately, it was necessary to select the tests to calibrate the material parameters and the tests on which the blind simulations would be made. This distinction is important for assessing the criticality of the model in the predictive phase.

Consequently, the standard oedometric tests presented in Ravera et al. (2021) have been used to define the elastic parameters. As reported by Mortara (2001), the normal elastic stiffness K_n is the ratio of the oedometric modulus to the interface thickness. $E_{oed} \cong 3000$ kPa was defined as the average value of the two tests in the range of the normal stress which was simulated later in the predictive phase of the model (125–250 kPa). For the interface thickness no direct measurement was possible. In previous studies, researchers evaluated the interface thickness using various techniques (DeJong et al., 2003; Fakharian & Evgin, 1997). However, these studies involved granular soil, and the interface thickness was usually defined with reference to the grain size; it is impossible to adopt the same criteria in the case of fine-grained soil, where the cohesion also plays a role. In the case of granular soil, the observed interface thickness is in the range of 1–3 mm. For fine-grained soil Thakur (2007) and Thakur (2011) measured the thickness in the range of 3–4 mm. Vardoulakis (2002b) and Vardoulakis (2002a) estimated the thickness in clay to be 1.4 mm based on the observations made by Morgenstern and Tchalenko (1967). Moore and Rowe (1988) assumed the thickness in clay to be in the range of 0.1–20 mm.

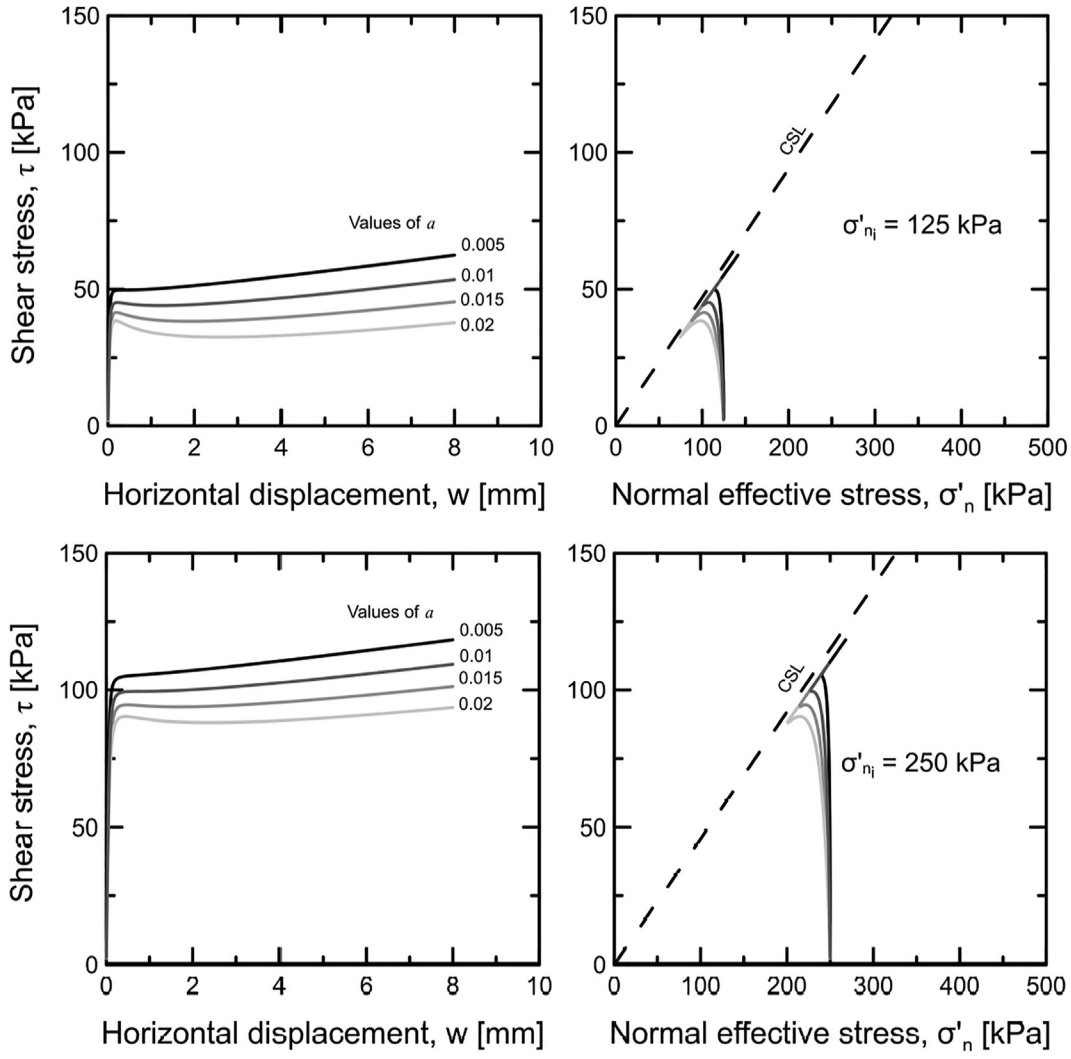

Fig. 5. Sensitivity analysis results for the parameter a.

Alonso et al. (2010) observed a thickness of 3–5 mm. Chakraborty et al. (2013) assumed a 2 mm thickness in clay in their numerical simulation. In this study, at the end of the test, a layer of fine material adhering to the concrete above which the slip occurred was observed. Therefore, the interface thickness was observed to be $s = 2$ mm. However, the precise quantification of the thickness of the interface is a delicate process (Pra-ai & Boulon, 2017) that remains an issue of debate within the scientific community. C_k was set to 1 as by Ghionna & Mortara (2002).

The CNL clay-concrete interface tests at ambient temperature performed by Di Donna et al. (2016) were used to establish the plastic parameters (μ, k_p, a). A value of $\varphi'_{cv} = 25°$ has been reported for the interface CNL interface test, corresponding to $\mu = tan\varphi'_{cv} = 0.47$. k_p is the limiting value of the stress ratio. The test results indicated that k_p was 0.442. As this value is derived from an interpretation of the experimental data, there are other defensible values of the parameter, as indicated by the results on the (w, τ) plane. Closely examining the mathematical formulation of the model reveals that the volumetric response depends on the relative values of k_p and μ. Thus, the volumetric response derived from the test is an important guide for the definition of the parameter. In this case, continuing volumetric compression (as failure is approached) has been observed. Thus, $k_p < \mu$ is considered appropriate. However, considering the uncertainty in the choice related to the subjectivity of the modeller, a sensitivity analysis of the parameter was performed, and the results are presented in Fig. 4. The stress path was not significantly affected before failure. The sensitivity of the response was noticed after the critical state line was reached. The difference was closely related to the volumetric behaviour of the material. Therefore, the information obtained from the CNL test (whether the material contracts or dilates) was important for the definition of this parameter. The sensitivity to this parameter is a potential limitation in the confidence of the model. This limitation indicates some of the deficiencies associated with the simplicity of the model that would need to be rectified if it were to be used for analyses where the need for accurate representation justifies an increase in modelling complexity. The last parameter is a, i.e. a soil constant that scale

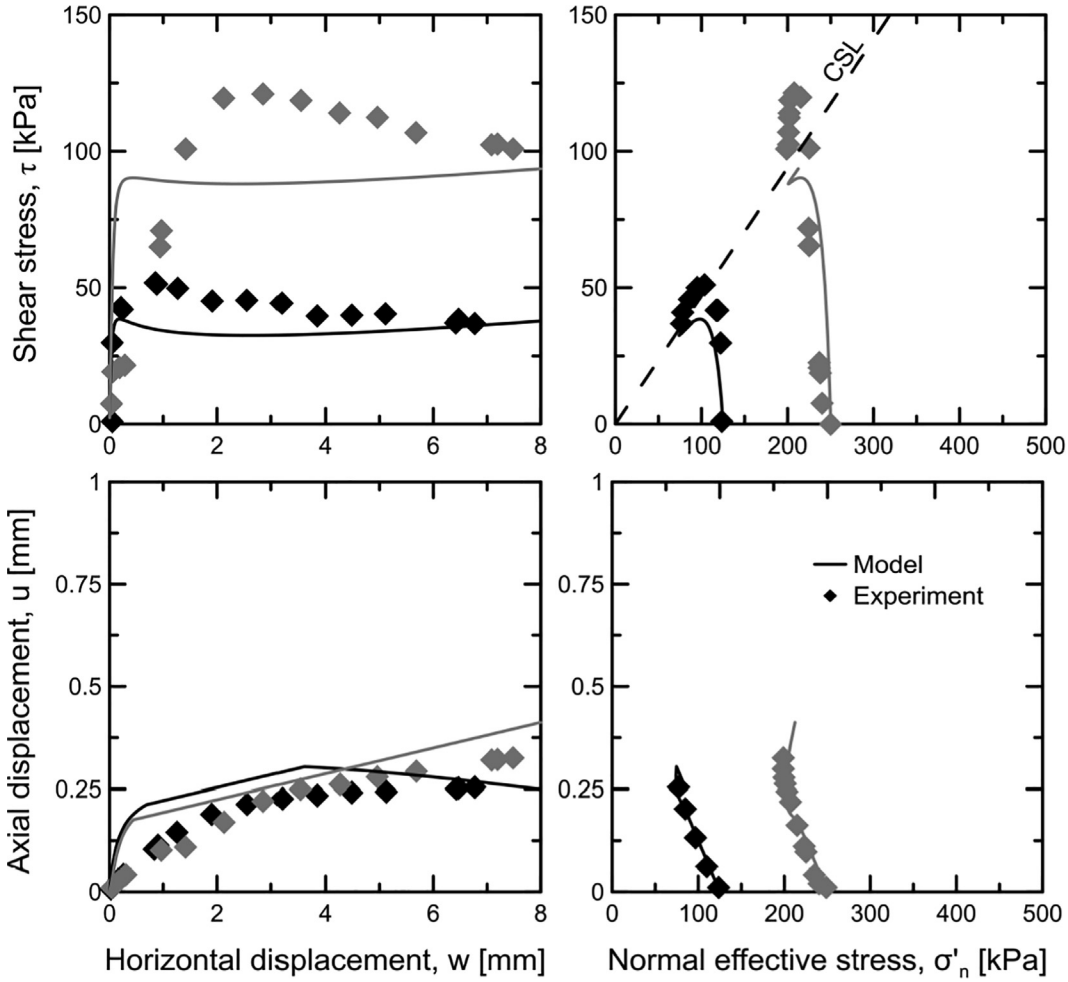

Fig. 6. Comparisons between the experimental results and the model predictions.

the plastic displacement. $a = 0.02$ is the tangential displacement required to reach a stress ratio of 70% of the limiting value. A sensitivity analysis was also performed for this parameter to investigate its effect on the prediction results. The observations were similar to those in the previous case, but with a less marked effect. As shown in Fig. 5, in the range analysed, the overall response changed only moderately as the parameter value changed. Table 1 presents the calibrated parameters. An important feature of the model is that only standard CNL tests and standard oedometric tests are required for the derivation of the parameters. In particular, a minimum of three monotonic CNL tests and one oedometer are sufficient to determine the parameters.

4.2.2. Validation tests

The experimental tests and model predictions were compared with reference to the tests described in the *Rheological evidences* section of this paper.

Fig. 6 presents comparisons between the experimental data obtained in the CNS tests, where thermal cycles were applied (CNS T with reference to Fig. 2), and predicted curves. Satisfactory agreement between the model predictions and experimental data is observed, particularly for the prediction of the overall response (rather than detailed modelling of specific aspects). Some of the deficiencies are associated with the simplicity of the model. However, the (σ'_n, τ) plane is the plane of greatest interest in foundation design, because the failure envelope is identified. The stress path that leads to failure was accurately predicted by providing important information about the evolution of the process in the pre-failure phase. The sensitivity of the response was noticed after the critical state line was reached. In practice, pre-peak response may be adequate since working loads are not intended to produce significant amounts of failure. The effectiveness of using an isothermal approach to model the results of the tests subjected to thermal cycles is illustrated. Given the limitations of the model due to its simplicity, however, it is highlighted that the model would have to be adjusted if it were to be used for analyses in which the need for accurate representation justifies an increase in the complexity of modelling.

5. Conclusion

The pile-soil interaction is a complex problem commonly encountered in geotechnical design, and the dominant factor to be considered for modelling this

phenomenon is the pile-soil interface. Indeed, the thin contact layer between the soil and the pile is strongly strained when the pile is loaded.

In this study, the soil-structure interface response was investigated, and the failure mechanism that is likely to be important in energy pile application was identified. The interface response of energy piles reproduced in the laboratory via cyclic thermal oedometric tests and cyclic thermal direct shear tests at a prescribed normal stiffness was analysed. The experimental results indicated that the interface behaviour for the energy pile when a cyclic temperature variation was applied was not different from that of conventional pile. This suggests that the mathematical models of the interface should have the same formal structure as the constitutive models normally employed for conventional piles. Raising the awareness of the modeler regarding the appropriate choices in constitutive modelling for finite-element or load-transfer analysis is of primary importance for the design of energy pile foundations. In the soil-structure interface behaviour, the use of constitutive laws in terms of stresses and strain (as in an elementary volume of soil) is prevented. The constitutive law should instead be expressed in terms of the stress vectors and relative displacements. An elastoplastic extended Mohr-Coulomb model with different variables (i.e., the relative tangential displacement corresponding to the shear strain) was proposed.

The proposed model requires a small number of parameters to completely describe the interface behaviour and the possibility to define them experimentally with commonly used soil test devices for geotechnical problems, which is a significant advantage for practical applications.

Acknowledgement

This work was supported by the Swiss National Science Foundation (financial support N. 200021_175500, Division II).

Appendix A - Algorithm for the implementation of the constitutive model

This appendix describes the algorithm used to implement the constitutive model. The algorithm presented refers to the works of Sloan (1987), Sloan et al. (2001) and Bosch LLufriu (2021) and has been adapted and modified for the specific application of this study.

6.1. Explicit modified Euler algorithm with error control

A.1 Enter with the initial stresses, $\boldsymbol{\sigma_0}$, the initial hardening parameter, k_0, the temperature, T, together with the displacement increment for the current load step $\Delta \boldsymbol{U}$

A.2 Compute the trial stress

$$\Delta \boldsymbol{\sigma}_e^{tr} = \mathbf{D}^{\mathbf{e}} \cdot \Delta \boldsymbol{U} \tag{A.1a}$$

$$\boldsymbol{\sigma}_e^{tr} = \boldsymbol{\sigma_0} + \Delta \boldsymbol{\sigma}_e^{tr} \tag{A.1b}$$

A.3 Check the yield condition

$$f_0 = f(\boldsymbol{\sigma_0}, k_0, T) \tag{A.2a}$$

$$f^{tr} = f(\boldsymbol{\sigma}_e^{tr}, k_0, T) \tag{A.2b}$$

a. if $f_0 > FTOL$ the stress state lies outside the yield surface therefore it is an illegal state.
b. if $f^{tr} \leq FTOL$ the stress state remains inside the yielding domain, hence the stress increment is purely elastic. Set $\boldsymbol{\sigma_f} = \boldsymbol{\sigma}_e^{tr}$ and $k_f = k_0$. Exit the algorithm.
c. if $f_0 < -FTOL$ and $f^{tr} > FTOL$ the increment causes a violation of the yield limit so there is a transition from elastic to plastic beahviour. It is necessary to find the intersection of the stress path with the yield surface. Compute the α factor that correspond to purely elastic deformation using Pegasus intersection scheme.
d. if $-FTOL \leq f_0 \leq FTOL$ and $f^{tr} > FTOL$ the increment is purely plastic, α is set equal to zero.

A.4 Compute the purely elastic portion of the increment

$$\Delta \boldsymbol{U}_e = \alpha \cdot \Delta \boldsymbol{U} \tag{A.3a}$$

$$\Delta \boldsymbol{\sigma}_e = \mathbf{D}^{\mathbf{e}} \cdot \Delta \boldsymbol{U} \tag{A.3b}$$

A.5 Compute the plastic portion of the increment

$$\Delta \boldsymbol{U_p} = (1 - \alpha) \cdot \Delta \boldsymbol{U} \tag{A.4}$$

A.6 Adopt a substepping procedure to solve the elastoplastic increments. Set $t = 0$ and $\Delta t = 1$. Initialise

$$\boldsymbol{\sigma_t} = \boldsymbol{\sigma_0} + \Delta \boldsymbol{\sigma_e} \tag{A.5a}$$

$$k_t = k_0 \tag{A.5b}$$

A.7 While $t < 1$ perform steps A.8–A.15

A.8 Compute $\Delta \boldsymbol{\sigma_i}$ and Δk_i for $i = 1, 2$ using:

$$\Delta \boldsymbol{\sigma_i} = \mathbf{D}^{\mathbf{e}} \cdot \Delta \boldsymbol{U_p} \cdot \Delta t - \Delta\lambda(\boldsymbol{\sigma_i}, k_i, T, \Delta \boldsymbol{\sigma_{e,i}}, \Delta t) \cdot \mathbf{D}^{\mathbf{e}} \cdot \boldsymbol{b}(k_i, T) \tag{A.6a}$$

$$\Delta k_i = \Delta\lambda(\boldsymbol{\sigma_i}, k_i, T, \Delta \boldsymbol{\sigma_{e,i}}, \Delta t) \cdot B(k_i, T) \tag{A.6b}$$

where

$$\Delta\lambda = \frac{\boldsymbol{a}^{\boldsymbol{T}} \cdot \Delta \boldsymbol{\sigma_e} \cdot \Delta t}{H + \boldsymbol{a}^{\boldsymbol{T}} \cdot \mathbf{D}^{\mathbf{e}} \cdot \boldsymbol{b}} \tag{A.7a}$$

$$H = -\frac{\partial f}{\partial k} \frac{\partial k^T}{\partial \boldsymbol{U^p}} \frac{\partial g}{\partial \boldsymbol{\sigma}} \tag{A.7b}$$

$$B = \frac{\partial k^T}{\partial \boldsymbol{U^p}} \frac{\partial g}{\partial \boldsymbol{\sigma}} \tag{A.7c}$$

$$\boldsymbol{a} = \frac{\partial f}{\partial \boldsymbol{\sigma}} \tag{A.7d}$$

$$\boldsymbol{b} = \frac{\partial g}{\partial \boldsymbol{\sigma}} \tag{A.7e}$$

and

$$\boldsymbol{\sigma_1} = \boldsymbol{\sigma_t}, k_1 = k_t \tag{A.8a}$$

$$\boldsymbol{\sigma_2} = \boldsymbol{\sigma_t} + \Delta \boldsymbol{\sigma_1}, k_2 = k_t + \Delta k_1 \tag{A.8b}$$

A.9 The new stress and hardening parameter are computed and stored temporarily

$$\boldsymbol{\sigma_{temp}} = \boldsymbol{\sigma_t} + \tfrac{1}{2} \cdot (\Delta \boldsymbol{\sigma_1} + \Delta \boldsymbol{\sigma_2}) \tag{A.9a}$$

$$k_{temp} = k_t + \frac{1}{2} \cdot (\Delta k_1 + \Delta k_2) \quad \text{(A.9b)}$$

A.10 The relative error for the current substep is computed as

$$R_{temp} = max\left(\frac{\|\Delta\boldsymbol{\sigma_1} - \Delta\boldsymbol{\sigma_2}\|}{2\|\boldsymbol{\sigma_{temp}}\|}, \frac{\|\Delta k_1 - \Delta k_2\|}{2\|k_{temp}\|}, \text{EPS}\right) \quad \text{(A.10)}$$

where EPS is the machine epsilon indicating the smallest relative error that may be computed.

A.11 If $R_{temp} > SSTOL$ the substep is refused and a smaller Δt is computed

$$q = max\left(0.9\sqrt{SSTOL/R_{temp}}, 0.1\right) \quad \text{(A.11)}$$

$$\Delta t \leftarrow \max\left(q\Delta t, \Delta t_{min}\right) \quad \text{(A.12)}$$

where Δt_{min} is the minimum substep size. Return to step A.8

A.12 If $R_{temp} \leq SSTOL$ the substepping is successful and the stresses and hardening parameter are updated

$$\boldsymbol{\sigma_t} = \boldsymbol{\sigma_{temp}} \quad \text{(A.13a)}$$

$$k_t = k_{temp} \quad \text{(A.13b)}$$

A.13 The updated stress state should be verified. If $|f(\boldsymbol{\sigma_t}, k_t, T)| > FTOL$ the stress state is not legal. A stress correction algorithm is applied in order to returning the stress state back to the yield surface.

A.14 The size of the next substep and new Δt are computed according to

$$t \leftarrow t + \Delta t \quad \text{(A.14a)}$$

$$q = min\left(0.9\sqrt{SSTOL/R_{new}}, 1.1\right) \quad \text{(A.14b)}$$

$$t \leftarrow q\Delta t \quad \text{(A.14c)}$$

Ensure the next step size is not smaller than the minimum step size and check that integration does not proceed beyond $t = 1$ by setting:

$$\Delta t \leftarrow max(\Delta t, \Delta t_{min}) \quad \text{(A.15a)}$$

$$\Delta t \leftarrow min(\Delta t, 1 - t) \quad \text{(A.15b)}$$

A.15 Exit with stresses $\boldsymbol{\sigma_f} = \boldsymbol{\sigma_t}$ and hardening parameter $k_f = k_t$ at the end of increment with $t = 1$.

The stresses $\boldsymbol{\sigma_f}$ are cheked in an iterative process to ensure that the CNS conditions are respected.

6.2. Pegasus intersection scheme

Pegasus procedure allows to define the scalar quantity α to solve the yield surface intersection.

A.16 Enter with the current stresses, $\boldsymbol{\sigma_0}$, the hardening parameter, k_0, the temperature, T, together with the displacement increment for the current load step $\Delta\boldsymbol{U}$.

A.17 Initialise the parameters

$$\alpha_0 = 0 \quad \text{(A.16a)}$$

$$\alpha_1 = 1 \quad \text{(A.16b)}$$

$$f^{new} = 1 \quad \text{(A.16c)}$$

A.18 Compute the elastic stress increment

$$\Delta\boldsymbol{\sigma_e} = \mathbf{D^e} \cdot \Delta\boldsymbol{U} \quad \text{(A.17a)}$$

$$\boldsymbol{\sigma_{\alpha_0}} = \boldsymbol{\sigma_0} + (\alpha_0 \cdot \Delta\boldsymbol{\sigma_e}) \quad \text{(A.17b)}$$

$$\boldsymbol{\sigma_{\alpha_1}} = \boldsymbol{\sigma_0} + (\alpha_1 \cdot \Delta\boldsymbol{\sigma_e}) \quad \text{(A.17c)}$$

A.19 Compute

$$f_0 = f(\boldsymbol{\sigma_{\alpha_0}}, k_0, T) \quad \text{(A.18a)}$$

$$f_1 = f(\boldsymbol{\sigma_{\alpha_1}}, k_0, T) \quad \text{(A.18b)}$$

A.20 While $|f^{new}| > FTOL$ and N° iterations $< MAXITS$ calculate

$$\alpha = \alpha_1 - f_1 \cdot \frac{\alpha_1 - \alpha_0}{f_1 - f_0} \quad \text{(A.19)}$$

A.21 Set

$$\boldsymbol{\sigma^{new}} = \boldsymbol{\sigma_0} + (\alpha \cdot \Delta\boldsymbol{\sigma_e}) \quad \text{(A.20a)}$$

$$f^{new} = f(\boldsymbol{\sigma^{new}}, k_0, T) \quad \text{(A.20b)}$$

a. If $|f^{new}| \leq FTOL$ return α
b. If $f^{new} \cdot f_0 < 0$ set $\alpha_1 = \alpha_0$ and $f_1 = f_0$
c. Else set $f_1 = f_1 \cdot \frac{f_0}{f_0 + f^{new}}$

A.22 Set $\alpha_0 = \alpha$ and $f_0 = f^{new}$

A.23 If the convergence is not achieved after $MAXITS$ iterations, print an error message and stop.

6.3. Yield surface correction scheme

The use of an explicit integration does not guarantee that the stress point lies on the yield surface at the end of an integration step. To correct the stress state to the yield surface:

A.24 Enter with uncorrected stress $\boldsymbol{\sigma_t}$, hardening parameter, k_t and the temperature T.

A.25 While N° iterations $< MAXITS$ compute:

$$\Delta\lambda = \frac{f_0(\boldsymbol{\sigma_t}, k_t, T)}{H(\boldsymbol{\sigma_t}, k_t, T) + \boldsymbol{a}^T(k_t) \cdot \mathbf{D^e} \cdot \boldsymbol{b}(k_t, T)} \quad \text{(A.21)}$$

A.26 Correct the stress and hardening parameter

$$\boldsymbol{\sigma_{corr}} = \boldsymbol{\sigma_t} - \Delta\lambda(\boldsymbol{\sigma_t}, k_t, T) \cdot \mathbf{D^e} \cdot \boldsymbol{b}(k_t, T) \quad \text{(A.22a)}$$

$$k_{corr} = k_t + \Delta\lambda(\boldsymbol{\sigma_t}, k_t, T) \cdot \mathbf{D^e} \cdot B(k_t, T) \quad \text{(A.22b)}$$

A.27 Compute

$$f_1 = f(\boldsymbol{\sigma_{corr}}, k_{corr}, T) \quad \text{(A.23)}$$

a. If $|f_1| > |f_0|$

$$\Delta\lambda = \frac{f_0(\boldsymbol{\sigma_t}, k_t, T)}{\boldsymbol{a}^T(k_t) \cdot \boldsymbol{a}(k_t)} \quad \text{(A.24a)}$$

$$\boldsymbol{\sigma_{corr}} = \boldsymbol{\sigma_t} - \Delta\lambda(\boldsymbol{\sigma_t}, k_t, T) \cdot \boldsymbol{a}(k_t) \quad \text{(A.24b)}$$

$$k_{corr} = k_t \quad \text{(A.24c)}$$

b. If $|f_1| < FTOL$ exit the algorithm with $\boldsymbol{\sigma_{corr}}$ and k_{corr}.

A.28 Set $\boldsymbol{\sigma_t} = \boldsymbol{\sigma_{corr}}$ and $k_t = k_{corr}$.

A.29 If convergence is not achieved print an error message and stop.

References

Alonso, E.E., Pinyol, N.M., Puzrin, A.M., 2010. Geomechanics of FAILURES. Springer Science & Business Media, Advanced topics.

Bosch LLufriu, J. A. Studies on the Mechanical Evolution of Compacted Bentonite Subjected to Environmental Actions. PhD thesis (EPFL, 2021).

Boulon, M., 1989. Basic features of soil structure interface behaviour. Comput. Geotech. 7 (1–2), 115–131.

Boulon, M., Foray, P. (1986). Physical and numerical simulation of lateral shaft friction along offshore piles in sand. In: Proc., 3rd Int. Conf. on Numerical methods in offshore piling (pp. 127-147). Institut Francais du Petrol, Nantes, France.

Boulon, M., Nova, R., 1990. Modelling of soil-structure interface behaviour a comparison between elastoplastic and rate type laws. Comput. Geotech. 9 (1–2), 21–46.

Boulon, M., Garnica, P., Vermeer, P.A., 1995. Soil-structure interaction: FEM computations. Stud. Appl. Mech. 42, 147.

Burghignoli, A., Desideri, A., Miliziano, S., 2000. A laboratory study on the thermomechanical behaviour of clayey soils. Can. Geotech. J. 37 (4), 764–780.

Cekerevac, C., Laloui, L., 2004. Experimental study of thermal effects on the mechanical behaviour of a clay. Int. J. Numer. Anal. Meth. Geomech. 28 (3), 209–228.

Chakraborty, T., Salgado, R., Basu, P., Prezzi, M., 2013. Shaft resistance of drilled shafts in clay. J. Geotech. Geoenviron. Eng. 139 (4), 548–563.

DeJong, J.T., Randolph, M.F., White, D.J., 2003. Interface load transfer degradation during cyclic loading: a microscale investigation. Soils Found. 43 (4), 81–93.

DeJong, J.T., White, D.J., Randolph, M.F., 2006. Microscale observation and modeling of soil-structure interface behavior using particle image velocimetry. Soils Found. 46 (1), 15–28.

Di Donna, A., Ferrari, A., Laloui, L., 2016. Experimental investigations of the soil–concrete interface: physical mechanisms, cyclic mobilization, and behaviour at different temperatures. Can. Geotech. J. 53 (4), 659–672.

Fakharian, K., Evgin, E., 1997. Cyclic simple-shear behavior of sand-steel interfaces under constant normal stiffness condition. J. Geotech. Geoenviron. Eng. 123 (12), 1096–1105.

Feligha, M., Hammoud, F., Belachia, M., Nouaouria, M.S., 2016. Experimental in vestigation of frictional behavior between cohesive soils and solid materials using direct shear apparatus. Geotech. Geol. Eng. 34 (2), 567–578.

Fleming, K., Weltman, A., Randolph, M., Elson, K., 2008. Piling Engineering. CRC Press.

Ghahremannejad, B. (2003). Thermo-mechanical behaviour of two reconstituted clays. Ph. D Thesis.

Ghionna, V.N., Mortara, G., 2002. An elastoplastic model for sand–structure interface behaviour. Géotechnique 52 (1), 41–50.

Graham, J., Tanaka, N., Crilly, T., Alfaro, M., 2001. Modified Cam-Clay modelling of temperature effects in clays. Can. Geotech. J. 38 (3), 608–621.

Hueckel, T., Pellegrini, R., 1989. Modeling of thermal failure of saturated clays. International Symposium on Numerical Models in Geomechanics. 3 (NUMOG III), pp. 81–90.

Hueckel, T., Baldi, G., 1990. Thermoplasticity of saturated clays: experimental constitutive study. J. Geotech. Eng. 116 (12), 1778–1796.

Laloui, L., Rotta Loria, A.F., 2019. Analysis and Design of Energy Geostructures: Theoretical Essentials and Practical Application. Academic Press.

Lancellotta, R., Ruiz, J.C., 1999. Fondazioni. McGraw-Hill.

Li, C., Kong, G., Liu, H., Abuel-Naga, H., 2019. Effect of temperature on behaviour of red clay–structure interface. Can. Geotech. J. 56 (1), 126–134.

Littleton, I., 1976. An experimental study of the adhesion between clay and steel. J. Terramech. 13 (3), 141–152.

Maghsoodi, S., Cuisinier, O., Masrouri, F., 2020. Thermal effects on mechanical behaviour of soil–structure interface. Can. Geotech. J. 57 (1), 32–47.

Moore, I.D., Rowe, R.K., 1988. Numerical models for evaluating progressive failure in earth structures—a review. Comput. Geotech. 6 (3), 217–239.

Morgenstern, N.R., Tchalenko, J.S., 1967. Microscopic structures in kaolin subjected to direct shear. Geotechnique 17 (4), 309–328.

Mortara, G., 2001. An elastoplastic model for sand-structure interface behaviour under monotonic and cyclic loading. Politecnico di Torino, Phd thesis.

Ovando-Shelley, E., 1995. Direct shear tests on Mexico City clay with reference to friction pile behaviour. Geotech. Geol. Eng. 13 (1), 1–16.

Potyondy, J.G., 1961. Skin friction between various soils and construction materials. Geotechnique 11 (4), 339–353.

Poulos, H.G., 2017. Tall Building Foundation Design. CRC Press.

Poulos, H.G., Davids, A.J., 2005. Foundation design for the emirates twin towers, Dubai. Can. Geotech. J. 42 (3), 716–730.

Pra-ai, S., Boulon, M., 2017. Soil–structure cyclic direct shear tests: a new interpretation of the direct shear experiment and its application to a series of cyclic tests. Acta Geotech. 12 (1), 107–127.

Randolph, M.F., 2003. Science and empiricism in pile foundation design. Géotechnique 53 (10), 847–875.

Ravera, E., Sutman, M., Laloui, L., 2021. Cyclic thermomechanical response of fine grained soil- concrete interface for energy piles applications. Can. Geotech. J. 99 (999), 1–15.

Robinet, J.C., Pasquiou, A., Jullien, A., Belanteur, N., Plas, F., 1997. Expériences de laboratoire sur le comportement thermo-hydro-mécanique de matériaux argileux remaniés gonflants et non gonflants. Rev. Fr. Géotech. 81, 53–80.

Rotta Loria, A.F., Coulibaly, J.B., 2020. Thermally induced deformation of soils: a critical overview of phenomena, challenges and opportunities. Geomech. Energy Environ. 25. https://doi.org/10.1016/j.gete.2020.100193 100193.

Shakir, R.R., Zhu, J., 2009. Behavior of compacted clay-concrete interface. Front. Arch. Civ. Eng. China 3 (1), 85–92.

Sloan, S.W., 1987. Substepping schemes for the numerical integration of elastoplastic stress–strain relations. Int. J. Numer. Meth. Eng. 24 (5), 893–911.

Sloan, S.W., Abbo, A.J., Sheng, D., 2001. Refined explicit integration of elastoplastic models with automatic error control. Eng. Comput.: Int. J. Comput.-Aid. Eng. 18 (1–2), 121–194.

Taylor, D.W. (1948). Fundamentals of soil mechanics (Vol. 66, No. 2, p. 161). LWW.

Thakur, V. (2007). Strain localization in sensitive soft clays. PhD thesis. NTNU, Trondheim.

Tabucanon, J.T., Airey, D.W., Poulos, H.G., 1995. Pile skin friction in sands from constant normal stiffness tests. Geotech. Test. J. 18 (3), 350.

Thakur, V., 2011. Numerically observed shear bands in soft sensitive clays. Geomech. Geoeng.: Int. J. 6 (2), 131–146.

Tsubakihara, Y., Kishida, H., 1993. Frictional behaviour between normally consoli dated clay and steel by two direct shear type apparatuses. Soils Found. 33 (2), 1–13.

Vardoulakis, I., 2002a. Steady shear and thermal run-away in clayey gouges. Int. J. Solids Struct. 39 (13-14), 3831–3844.

Vardoulakis, I., 2002b. Dynamic thermo-poro-mechanical analysis of catastrophic landslides. Geotechnique 52 (3), 157–171.

Wood, D.M., 2004. Geotechnical Modelling. CRC Press.

Yavari, N., Tang, A.M., Pereira, J.M., Hassen, G., 2016. Effect of temperature on the shear strength of soils and the soil–structure interface. Can. Geotech. J. 53 (7), 1186–1194.

Yazdani, S., Helwany, S., Olgun, G., 2019. Influence of temperature on soil–pile interface shear strength. Geomech. Energy Environ. 18, 69–78.